Polarized Phase-Sensitive-Fluorescence Image Correlation Spectroscopy

Andrew H. A. Clayton *

Posted Date: 4 March 2026

doi: 10.20944/preprints202603.0322.v1

Keywords: image correlation spectroscopy; fluorescence lifetime imaging microscopy; polarization

 doi:10.20944/preprints202603.0322.v1

Article

Polarized Phase-Sensitive-Fluorescence Image Correlation Spectroscopy

Andrew H. A. Clayton

Optical Sciences Centre, Department of Physics and Astronomy, School of Science, Computing and Emerging Technologies, Swinburne University of Technology, Hawthorn, Melbourne, Australia; aclayton@swin.edu.au

Abstract

Molecular interactions underpin the functioning of the living cell. Molecules exist in distinct quaternary structural forms, associate with molecular partners in signaling cascades, form transient quinary interactions, localize in membrane domains, and cluster in membrane-less condensates. Measuring the concentration, size, and dynamics of these molecular assemblies remains an enduring biophysical challenge, particularly in cells, where heterogeneity is the rule rather than the exception. Orthogonal signals derived from fluorescence lifetime, fluorescence fluctuations, and fluorescence polarization provide valuable metrics for probing interactions and environments, concentration and size, as well as rotational dynamics, respectively. This paper combines fluorescence lifetime imaging microscopy with image correlation analysis and polarization to determine the concentrations, brightness, lifetime, and rotational correlation time of different fluorescent states. A two-population model is examined as a prototypical example of a heterogenous system. The analysis is illustrated on a simple fluorescence model system, where cluster densities, relative brightnesses, lifetimes and rotational correlation times are extracted.

Keywords: image correlation spectroscopy; fluorescence lifetime imaging microscopy; polarization

1. Introduction

The living cell represents a fascinating entity for biophysical enquiry. At the molecular scale proteins, nucleic acids, carbohydrates and lipids form networks of transient interactions, polymers, membranes, organelles, membrane-less condensates and machines capable of carrying out the instructions in the genetic blueprint. To function, molecules must move. Making sense of these thermally driven (non)equilibrium motions and interactions is a challenge, akin to the partially stochastic, partially random motions of people in a metropolis. At the same time the invention of techniques such as fluorescence correlation spectroscopy [1] allows the experimentalist to extract quantitative information from the apparent noisy behavior of molecules in time observed through a tiny window (diffraction-limited excitation volume). If we instead take a wide-field snapshot from a population of these molecules in a single moment of time, we can still obtain information from the fluctuations in space. Analysis of fluctuations from an image is referred to image correlation spectroscopy [2–9]. The power of images is the very large number of fluctuations that can be obtained in parallel.

Fluorescence itself is a phenomenon rich with information. The average time a molecule spends in the excited state or fluorescence (detected) lifetime, typically nanoseconds, is sensitive to molecular environment. Lifetime measurements become especially valuable in methods such as Foerster Resonance Energy Transfer where energy transfer from an initially excited donor molecule to a nearby (1-10nm) acceptor molecule produce a characteristic proximity-dependent reduction in fluorescence lifetime [10–16]. Fluorescence polarization (or anisotropy) [17–29] is a dimension of fluorescence which is sensitive to rotational motion. Excitation with plane-polarized light produces an instantaneous anisotropic distribution of excited-state molecules with transition dipole moments aligned with the electric-field vector of the exciting light. Detection of the parallel and/or

 doi:10.20944/preprints202603.0322.v1

perpendicular components of the emission after polarized excitation reflects the ensuing change in orientation of the ensemble as the orientations become randomized through collisions with solvent molecules.

In this paper, we wish to use image correlation spectroscopy in a novel way. By combining image correlation spectroscopy, with lifetime imaging microscopy and polarized excitation/detection the goal is to determine the density, brightness, lifetime and rotational correlation time of different species in an image. The key is the use of phase-sensitive detection in fluorescence lifetime imaging microscopy [10]. In wide-field frequency-domain FLIM, excitation is in the form of sinusoidally-modulated light at radiofrequencies (typically 40MHz). The fluorescence is then detected with a 2D intensifier-camera which is gain-modulated at the same frequency as the fluorescence. By progressively shifting the phase of the detector with respect to the fluorescence, particles with certain lifetime can be in-phase or out-of-phase with the detector. In this manner particles with certain lifetimes can be optically suppressed or enhanced in the image. By using image correlation spectroscopy to measure the cluster density of particles as a function of detector phase, the densities of particles with different lifetimes can then be inferred [30]. When polarized excitation and orthogonal polarized detection is added to the lifetime measurement, fluorescence from slow rotating species will be selectively diminished with respect to fast rotating species, while species that rotate comparably with the excited-state lifetime will be further delayed in phase. By comparing the phase-dependent cluster densities in the unpolarized case with the polarized situation, information on rotational correlation times of different species should, in principle, be able to be extracted.

The paper is organized as follows. In the theory section we present the key equations underpinning the polarized phase sensitive fluorescence image correlation spectroscopy method. In the results section we then present simulations to show the sensitivity of the method. To provide a test bed for this novel ICS variant, we consider a two-population model as the simplest case for a heterogenous system. Mimicking a receptor system in membrane domains, or a protein in different oligomeric states, we allow one population to be brighter than the other population. We simulate different combinations of lifetimes and correlation times. We then present measurements of phase sensitive images with unpolarized excitation and polarized excitation of a model fluorescent system consisting of bright beads. In the context of a two-state model, we were able to recover the cluster densities, relative brightness, lifetimes and rotational correlation times of the two states. In the discussion section we discussed the advantages and limitations of the new method.

2. Materials and Methods

Polarization and phase-dependent images were collected using a commercial frequency-domain FLIM system (LIFA, Lambert Instruments, Groningen, the Netherlands) mounted on a research grade microscope (Model Ti, Nikon, Japan). Excitation was provided by a 474nm LED modulated at 35MHz which was passed through a linear polarizer (Thor Labs, USA) and focused through a 4X objective lens (Nikon, Japan; NA=0.1). Fluorescence was observed through a hyperspectral imaging system (His-400; Gooch & Housego, Orlando, Florida, USA) set to 520nm (20nm width) and imaged using an intensifier-CCD camera. The photocathode of the image intensifier was modulated at the same frequency as the excitation (35MHz) but with a square-wave profile to increase instrument modulation depth. Twelve phase images were recorded in pseudo-random order and over a full phase cycle under computer control using LIFA software (Lambert Instruments, the Netherlands). Instrumental correction factors were determined by using rhodamine 6G in distilled water (lifetime=4.1 ns) as the reference.

3. Theory

The theory for phase-sensitive fluorescence image correlation spectroscopy was presented in a previous publication [30]. For the sake of completeness, we recap the most relevant formulae here and present the extension to polarized excitation/detection.

 doi:10.20944/preprints202603.0322.v1

Recalling that in our experimental fluorescence lifetime imaging microscopy set-up, fluorophores in an object are excited with intensity-modulated excitation (sinusoidal) and the fluorescence detected by an image-intensifier-camera combination whose sensitivity is also (square wave) modulated at the same frequency as the excitation. In this homodyne mode of operation, fluorescence images are recorded at different phase settings of the detector over a full cycle of 0 to 2pi. If we plot the average image intensity I as a function of detector phase ϑ, the intensity profile follows a cosine-like function, see Equation (1),

$$I(\vartheta)=I_0(1+m\cos(\Phi-\vartheta)) \quad (1)$$

In the right-hand side of Equation (1), m is the modulation and Φ is the phase of the fluorescence signal, both corrected for the instrument response, and I_0 is the average emission intensity. The modulation and phase values are related to the lifetime of the excited state of the fluorescence. If $m=\cos(\Phi)$, then a unique lifetime may be determined from the phase or modulation values. If $m<\cos(\Phi)$ then the excited-state decay process is more complex.

In the phase-sensitive fluorescence image correlation spectroscopy technique [30], image correlation spectroscopy analysis [4–7] is applied to fluorescence images recorded as a function of phase. Image correlation spectroscopy analysis uses the spatial autocorrelation function to compute the autocorrelation as a function of spatial lag. The autocorrelation at zero lag is related to the cluster density of particles. The cluster is a fluorescent particle and could be a monomer, dimer or any sized fluorescent entity. The autocorrelation function g(dx,dy) as a function of spatial lag (dx,dy) is defined in Equation (2).

$$g(dx,dy)=\langle I(x,y)\, I(x+dx,y+dy)\rangle/\langle I(x,y)\rangle^2-1 \quad (2)$$

In Equation (2), I(x,y) represents the image with intensity I at pixel location (x,y). The reciprocal of g(0,0) is the cluster density of CD in units cluster per beam area.

We now examine the microscopic factors behind the fluorescence image. Fluorescent entities are treated as particles with a brightness B (units: intensity/cluster) and dispersed with a cluster density CD (units: clusters per beam area). If there is only one type of particle, then image correlation spectroscopy [4–7] analysis (spatial autocorrelation analysis) of the image will deliver the cluster density and brightness of that particle. For a heterogenous system, image correlation spectroscopy analysis will deliver an average cluster density <CD> as a weighed sum of the individual particle characteristics. To be more specific,

$$\langle CD\rangle=(CD_1B_1+CD_2B_2+\ldots)^2/(CD1(B_1^2)+CD_2(B_2^2)+\ldots) \quad (3)$$

In Equation (3), CD_1 is the cluster density of population 1 and B_1 is the brightness of population 1, CD_2 is the cluster density of population 2 and B_2 is the brightness of population 2 and so on.

In phase sensitive fluorescence ICS [30], image correlation analysis [4–7] is applied to each image in the phase stack. We can re-write equation (3) as,

$$\langle CD\rangle(\vartheta)=(CD_1B(\vartheta)_1+CD_2B(\vartheta)_2+\ldots)^2/(CD_1B(\vartheta)_1^2+CD_2B(\vartheta)_2^2+\ldots) \quad (4)$$

Where, the brightness, $B_i(\vartheta)$, is modulated with the phase, ϑ, of the detector according to,

$$Bi(\vartheta)=B_i(1+m\cos(\Phi_i-\vartheta)) \quad (5)$$

As noted in our previous publication [30], if all particles have the same lifetime (phase), then the cluster density will be independent of the phase of the detector. However, if particles have different lifetimes, then the cluster density will be dependent on the phase of the detector. The output from the analysis of phase-sensitive ICS is the cluster density and brightness of particles with different lifetimes. The reader should refer to our previous paper [30] for examples of different types of cluster and lifetime distributions including bimodal (two-populations), Gaussian and Lorentzian lifetime distributions.

We now wish to consider the situation of fluorescence lifetime imaging microscopy performed with polarized excitation and perpendicular polarized detection. Depopulation of the excited state

 doi:10.20944/preprints202603.0322.v1

will produce a phase shift and demodulation, as discussed above. Under conditions of polarized excitation and perpendicular polarized detection, rotational motion and/or transfer of electronic energy will induce an additional change in phase and hypo modulate the emission [20]. We denote the resultant phase as Φ_{perp} and the modulation as m_{perp}. The brightness will also decrease depending on the rotational correlation time (ϕ) and the lifetime (τ).

The form of the average cluster density of the perpendicular-polarized component of the emission ($<CD>(\vartheta)_{perp}$) as a function of detector phase is analogous to the case of non-polarized excitation,

$$<CD>(\vartheta)_{perp}=(CD_1B(\vartheta)_{1perp}+CD_2B(\vartheta)_{2perp}+\ldots)^2/(CD_1B(\vartheta)_{1perp}^2+CD_2B(\vartheta)_{2perp}^2+\ldots) \quad (6)$$

Where, the brightness, $B_i(\vartheta)_{perp}$, is modulated with the phase, ϑ, of the detector according to,

$$B_i(\vartheta)_{perp}=B_{iperp}(1+m_{perp}\cos(\Phi i_{perp}-\vartheta)) \quad (7)$$

For a fluorescent particle with anisotropy, r, the brightness of the particle is reduced with crossed polarization. The ratio of B_{perp} to B is given by equation (8).

$$B_{perp}/B=(1/3)(1-r) \quad (8)$$

The steady-state anisotropy is related in turn to the lifetime and correlation time by the Perrin-Jablonski equation,

$$r=r_0/(1+(\tau/\phi)) \quad (9)$$

where r_0 is the fundamental anisotropy (in the absence of rotation). The perpendicular-polarized modulation and the perpendicular-polarized phase are complex functions of lifetime, correlation time, fundamental anisotropy and optical modulation frequency and can be calculated from formulae published elsewhere [20,25,28,29]. For the interested reader we present formulae in the Appendix A. In the next section we investigate how different particle distributions influence the CD and CD_{perp} versus phase plots.

4. Results

In this section we investigate different particle distributions, specifically examining different links between lifetime and correlation time. We begin with a simple system containing two populations of particles. One population with density CD_1=0.40 clusters/beam area and B=3 (population 1) and a second population of particles with CD_2=0.39 clusters/beam area and B=1 (population 2). The results allow some qualitative observations to be made.

(i) Single lifetime and single correlation time.

Figure 1 depicts a simulation of with all particles having a lifetime of 3.6ns and a rotational correlation time of 5ns. Despite the differences in particle densities and particle brightnesses between populations 1 and 2, the phase dependent cluster densities are independent of phase and polarization. This is because all particles have identical phase. The observed CD is not equal to the sum of CD_1 and CD_2 because population 1 with CD_1 is three times brighter than population 2 with CD_2. The conclusion from this simulation is that to have a CD that depends on phase you must have some heterogeneity in phase (originating from heterogeneity in lifetime and/or correlation time). As an aside, for a single lifetime, single correlation time system, use of the modulation and phase (Equation (1)) from the average image intensity phase stack can be combined with the analogous quantities under polarized excitation/perpendicular polarized detection, to extract the lifetime and correlation time using AB, polar or phasor plot [28,29].

 doi:10.20944/preprints202603.0322.v1

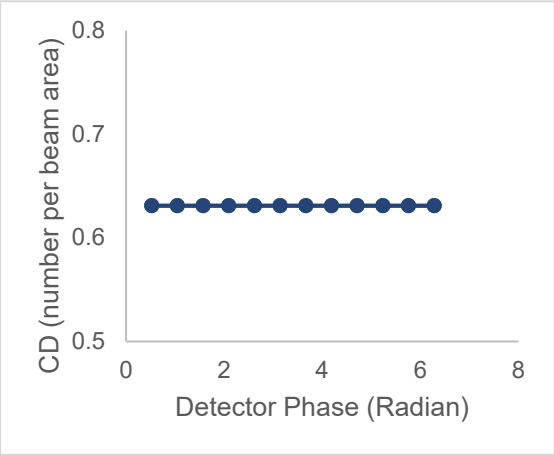

Figure 1. Polarized phase sensitive fluorescence ICS for 2 population model with identical lifetimes and identical correlation times (population 1 (CD_1=0.40 clusters/beam area; B=3, τ=20.2ns, ϕ=ϕ_1=5ns); population 2(CD_2=0.39 clusters/beam area, B=1, τ=20.2 ns, ϕ=ϕ_2=5ns)). Line with filled symbols represents the CD_{perp} versus phase for the condition specified above. Simulations were with an optical modulation frequency of 35MHz and a zero-time fundamental anisotropy r_0=0.4.

(ii) Single lifetime and two correlation times

We now examine the cases of population 1 (CD_1=0.40 clusters/beam area; B=3, τ=20.2ns) and population 2 (CD_2=0.39 clusters/beam area, B=1, τ=20.2ns) having distinct single correlation times, ϕ_1 (for population 1) and ϕ_2 (for population 2) but maintaining identical lifetimes. Figure 2 depicts simulations for different combinations of correlation times (filled symbols), together with the simulation for the unpolarized excitation (unfilled symbols). Rotational motion in both populations is seen to influence the CD_{perp} versus phase plots for the perpendicular polarized emission. While the unpolarized excitation plot is linear with gradient zero (horizontal), the polarized plots show a small level of curvature. However, the curvature is low with a coefficient of variation of less than 1%. The main effect of rotational motion is to produce an offset along the apparent CD axis, relative to the unpolarized case. Conditions which make population 1 polarized and population 2 relatively depolarized give rise to an enhancement in the CD_{perp} value (relative to the unpolarized case). Whereas conditions which make population 2 polarized and population 1 depolarized give rise to a reduction in CDperp value (relative to the unpolarized case). The curves show that distinction between different correlation time models involving pairs of correlation times can be made at least when the correlation times differ by order of magnitude.

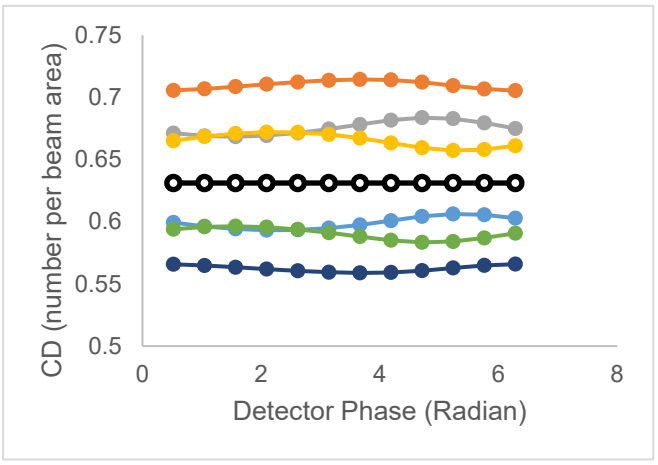

Figure 2. Polarized phase sensitive fluorescence ICS for 2 population models with identical lifetimes but different rotational correlation times (population 1 (CD_1=0.40 clusters/beam area; B=3, τ=20.2ns, ϕ=ϕ_1);

 doi:10.20944/preprints202603.0322.v1

2(CD_2=0.39 clusters/beam area, B=1, τ=20.2 ns, $\phi=\phi_2$)). Lines with filled symbols from top to bottom correspond to correlation time pairs (ϕ_1, ϕ_2) = (200,2), (200,20), (20,2), (2,20), (20,200), (2,200). Line with unfilled symbols corresponds to unpolarized excitation. Simulations were with an optical modulation frequency of 35MHz and a zero-time fundamental anisotropy r_0=0.4.

(iii) Two lifetimes and one correlation time

We now examine the cases of population 1 (CD_1=0.40 clusters/beam area; B=3, τ_1=3.6 ns) and population 2(CD_2=0.39 clusters/beam area, B=1, τ_2=20.2 ns) having distinct single lifetimes but maintaining shared, single rotational correlation times. Figure 3 depicts the CD_{perp} versus phase for different rotational correlation times. For the unpolarized case, the CD versus phase plot has a distinctive peak, owing to the difference in lifetimes of the two populations and the larger brightness of the short lifetime population. Rotational motion is seen to cause either broadening or peak splitting in the CD_{perp} versus phase plots. Broadening occurs for short (0.1 and 1 ns) and very long correlation times (20ns and 50ns) while peak spitting occurs with a rotational correlation time of 5ns and 10ns.

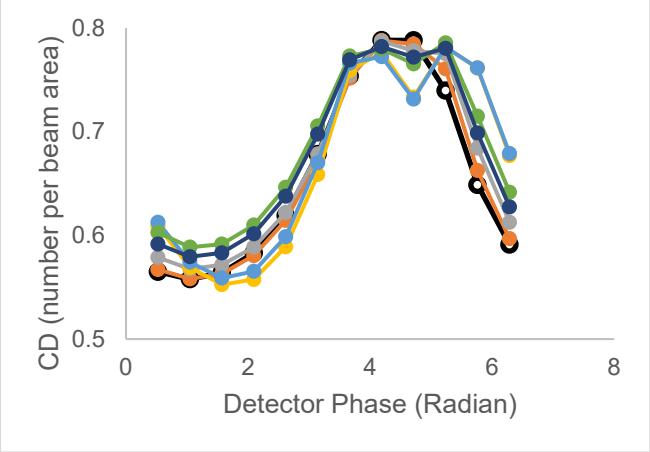

Figure 3. Polarized phase sensitive fluorescence ICS for 2 population models with distinct lifetimes but shared single rotational correlation times (population 1 (CD_1=0.40 clusters/beam area; B=3, τ=3.6ns, $\phi=\phi_1$); population 2(CD_2=0.39 clusters/beam area, B=1, τ=20.2 ns, $\phi=\phi_1$)). Lines with filled symbols from top to bottom at 6.28 radians correspond to correlation times (ϕ)=(10,20,50,1,0.1) in nanoseconds. Line with unfilled symbols corresponds to unpolarized excitation. Simulations were with an optical modulation frequency of 35MHz and a zero-time fundamental anisotropy r_0=0.4.

(iv) Two lifetimes and two correlation times (un-associated)

We now examine the cases of population 1 (CD_1=0.40 clusters/beam area; B=3, τ_1=3.6 ns) and population 2(CD_2=0.39 clusters/beam area, B=1, τ_2=20.2 ns) having distinct single lifetimes but now sharing the same rotational correlation times (with a 50% contribution of ϕ_1 and a 50% contribution of ϕ_2). Figure 4 depicts the CD versus phase for different value sets of ϕ_1 and ϕ_2 (0.36ns,2ns), (3.6ns,2ns), (3.6ns,20ns), (0.36ns,20ns), (36ns,2ns), (36ns,20ns).

For the unpolarized case, the CD versus phase plot has a distinctive peak, owing to the difference in lifetimes of the two populations and the larger brightness of the short lifetime population. As for the single correlation time case (above), rotational motion is seen to cause either broadening or peak splitting in the CD_{perp} versus phase plots.

 doi:10.20944/preprints202603.0322.v1

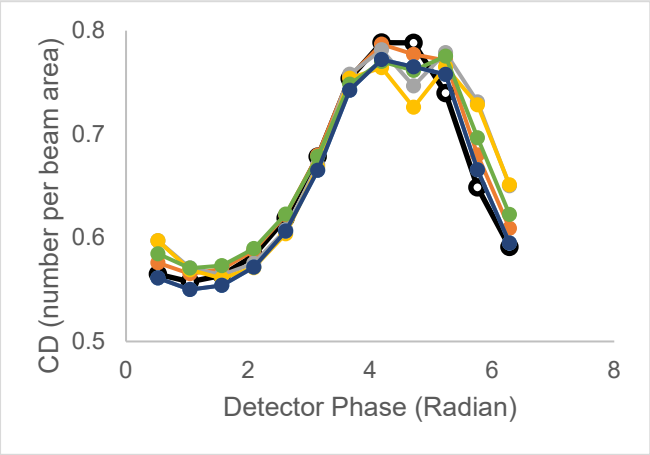

Figure 4. Polarized phase sensitive fluorescence ICS for 2 population model with distinct lifetimes but shared two-component rotational correlation times ((ϕ_1, ϕ_2)) (population 1 (CD_1=0.40 clusters/beam area; B=3, τ_1=3.6 ns); population 2 (CD_2=0.39 clusters/beam area, B=1, τ_2=20.2 ns). Lines with filled symbols from top to bottom at 4.7 radians correspond to correlation time pairs (ϕ_1, ϕ_2) in ns) = (0.36,2), (36,20), (3.6,2), (3.6,20). Line with unfilled symbols corresponds to unpolarized excitation. Simulations were with an optical modulation frequency of 35MHz and a zero-time fundamental anisotropy r_0=0.

(v) Two lifetimes and two correlation times (associated)

We now examine the cases of population 1 (CD_1=0.40 clusters/beam area; B=3, τ_1=3.6 ns) with distinct correlation time ϕ_1 and population 2 (CD_2=0.39 clusters/beam area, B=1, τ_2=20.2 ns) with correlation time ϕ_2. That is, an associative model.

Figure 5 depicts CD versus phase plots for different associative models. In the associative model peak narrowing, peak broadening and peak splitting is observed. However, there are also changes in the amplitude. Peak narrowing is accompanied by a decrease in peak amplitude and peak splitting is accompanied by an increase in amplitudes of the two peaks. By way of orientation the plot with largest splitting and highest amplitudes corresponds to ϕ_1=100τ_1=360 ns and ϕ_2=0.01τ_2=0.2ns. Whereas the plot with the single peak at the lowest amplitude corresponds to the ϕ_1=0.01τ_1=0.036 ns and ϕ_2=100τ_2 = 2000ns.

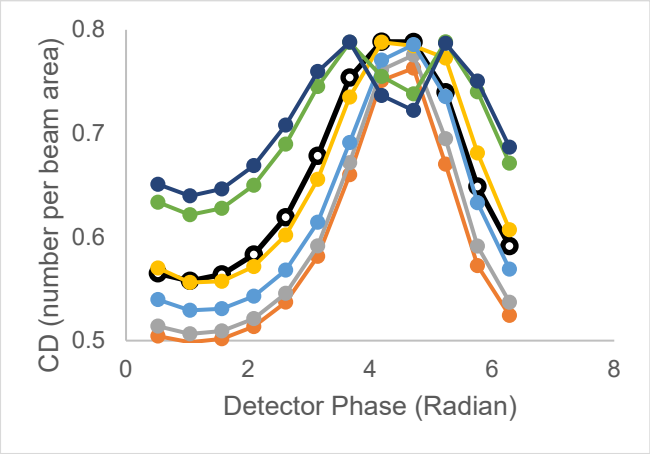

Figure 5. Polarized phase sensitive ICS for 2 population models with distinct lifetimes and associated distinct rotational correlation times (population 1 (CD_1=0.40; B=3, τ_1=3.6 ns); population 2 (CD_2=0.39, B=1, τ_2=20.2 ns). Lines with filled symbols from top to bottom at 6.28 radians correspond to lifetime-associated correlation times ($\tau_1 \rightarrow \phi_1$, $\tau_2 \rightarrow \phi_2$) = (360,0.2), (36,2),(3.6,20),(3.6,200),(0.36,200),(0.036,2000). Line with unfilled symbols corresponds to unpolarized excitation. Simulations were with an optical modulation frequency of 35MHz and a zero-time fundamental anisotropy r_0=0.

 doi:10.20944/preprints202603.0322.v1

From the simulations we can summarise the qualitative features of polarized phase-sensitive ICS simulations in the Table 1 below. In general, homogenous lifetimes and correlations times are predicted to produce CD (CD_{perp}) versus phase plots which are independent of phase, lifetime and correlation time. Single lifetimes but heterogenous correlation times produce CD_{perp} plots that depend on the rotational correlation times. Heterogenous lifetimes produce dips (previous work [30]) or peaks in CD with phase. Depending on how the rotational correlation times are coupled to the lifetimes (associative or non-associative) rotational motion can cause broadening, peak splitting and amplitude changes in the CD versus phase plots. These simulations provide some insights into the sorts of changes that might be anticipated where populations differ in brightness, lifetime and rotational correlation times, but of course are not intended to be exhaustive.

Table 1. Qualitative model-dependent features of CD versus phase and CD_{perp} versus phase plots for two populations of clusters. Population 1 clusters had a brightness of 3 and were dispersed at a cluster density of 0.39 clusters/beam area while population 2 had a brightness of 1 and a cluster density of 0.40 clusters/beam area. Numerical values of the lifetimes and correlation times are given in the previous figures.

Model	Lifetime	Correlation time	CD/CDperp
1 τ and 1 ϕ	τ	ϕ	CD is constant CD_{perp} is constant
1 τ and 2 ϕ	$\tau_1=\tau_2$	ϕ_1,ϕ_2	CD is constant $CD_{perp}=F(\phi_1,\phi_2)$
2 τ and 1 ϕ	τ_1,τ_2	ϕ	CD has peak CD_{perp} broad,split
2 τ and 2 ϕ (non-assoc)	τ_1,τ_2	ϕ_1,ϕ_2	CD has peak CD_{perp} broad,split
2 τ and 2 ϕ (assoc)	τ_1,τ_2	ϕ_1,ϕ_2	CD has peak CD_{perp} broad, split, and amplitude

(vi) Application to experimental sample.

To put into practice the ideas presented above, we require a sample which contains fluorescence fluctuations across an image. A test sample was created containing commercial fluorescent beads that were dropped onto a microscope slide and left to dry. Figure 6 depicts a surface plot (generated in FIJI) of a fluorescence image of the bead sample collected with a wide-field fluorescence microscope (LED excitation 470nm, emission filter centered 510nm) showing the anticipated punctate fluorescence from the beads.

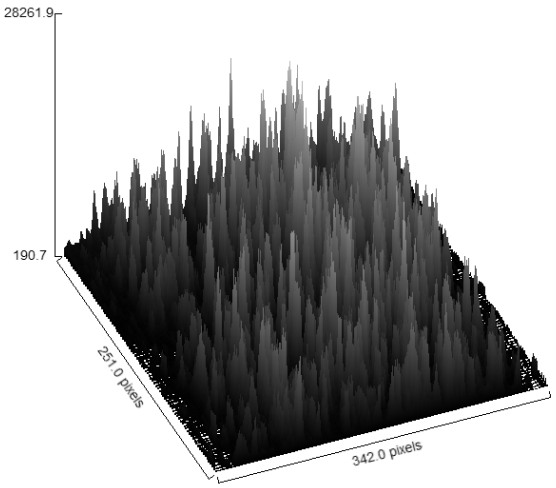

 doi:10.20944/preprints202603.0322.v1

Figure 6. 3D surface plot of a collection of fluorescent beads. Note the significant fluorescent fluctuations due to the fluorescent particles in the image. Images were acquired with 470nm excitation and emission collected through hyperspectral imaging device centered near 510nm (width:20nm). Note 3D surface plot is for qualitative visualization purposes only.

As part of the standard operation of our commercial wide-field frequency-domain microscope (LIFA, Lambert instruments, the Netherlands) phase-sensitive images were acquired at twelve different phases of the detector (optical modulation frequency, 35MHz, 12 phase steps over a 2pi radians), under computer control. One series was collected without excitation polarized (unpolarized excitation) and the other series was collected with excitation polarizer included in the excitation path of the microscope. Our hyperspectral imaging system (centre:520nm, width=20nm) has a polarizer set to the horizontal (perpendicular) and this serves as the analyzer in our microscope. Ten replicates of these image series were taken in total (10*12=120 phase-dependent images).

Phase-sensitive fluorescence images from the FLIM experiment were saved as raw images and then imported into FIJI for the image correlation analysis. For simplicity only the spatial autocorrelation at zero-lag was required for the analysis.

Figure 7 depicts the CD versus phase data (empty symbols) and the CD_{perp} versus phase data (filled symbols) extracted from the bead images.

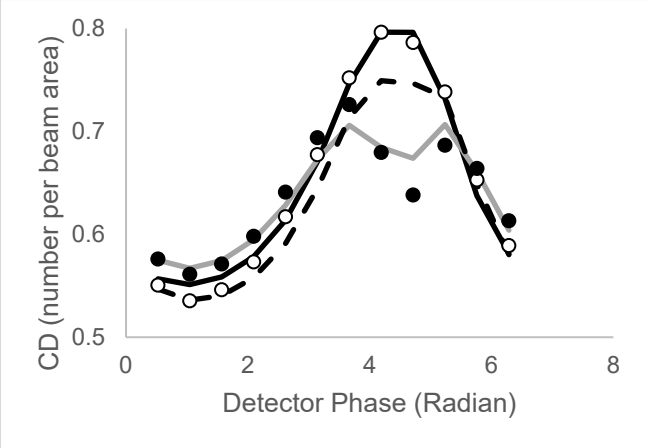

Figure 7. Polarized phase sensitive fluorescence ICS from fluorescence image of beads. Unfilled circles represent CD versus phase with unpolarized excitation and filled circles represent CD_{perp} versus detector phase with polarized excitation. Solid lines represent fits to specific models. See main text for details.

The CD versus phase has a clear dependence on detector phase with a trough near 1 radian of 0.53 clusters/beam area and a single peak near 4 radians close to 0.8 clusters/beam area. The significant dependence of CD on phase appears to rule out a single lifetime model and instead points to a heterogenous lifetime model (c/f Table 1 and Figures 1 and 2). The solid line in Figure 7 reveals the quality of fit to a two-population model for CD versus phase data, with parameters (population 1(CD_1=0.38; B_1=3, τ=3.9 ns); population 2(CD_2=0.42, B_2=1, τ=19.4 ns).). The CD_{perp} versus phase plot differs noticeably from the CD versus phase plot, especially with split peaks and reduced peak amplitudes. To fit the polarized phase-dependent CD data, lifetimes and brightness values were fixed to the values obtained from the unpolarized excitation dataset, while CD values were allowed to be rescaled (12% decrease). Different correlation time models were tested including common single correlation time, common two correlation times as well as an associative model. The dashed line in Figure 7 represents the fit to a common single correlation time model. The associative model produced a fit with a sum-of-squares that was a factor of 2 smaller than the other two other models tested. The solid line in Figure 7 reveals the fit to an associative model. In this model the 3.9ns bright clusters are rotationally immobile (ϕ_1=10000 ns) while the dimmer 20 ns clusters are completely and rapidly depolarized (ϕ_2=0.001 ns). An alternative model posits that everything is immobilized but the

 doi:10.20944/preprints202603.0322.v1

19ns clusters have a fundamental zero-time anisotropy close to zero (i.e., $r0_2$=0, ϕ_2=10000 ns). This model fits the data equally as well. The beads sample is a solid, dried sample and thus we would anticipate a rotationally constrained environment for the fluorophores in accordance with the latter interpretation. Qualitatively at least the bright clusters with lifetime close to 4ns are highly polarized in emission but the dim clusters with 20ns are depolarized in emission (either due to homo-transfer of electronic energy or possibly change in transition moment directions between absorption and emission). Further work is required to understand the photophysical origins of the apparently depolarized state.

A self-consistency test of the model can be made by comparing the measured cluster density in a conventional (unmodulated) fluorescence image of the beads with the calculated cluster density derived from the extracted brightness and cluster densities of the populations. The measured cluster density of an unmodulated image (i.e., image from summing the phase dependent images over a full cycle) was 0.629 clusters/beam area. This can be compared with the value of 0.623 clusters/beam area derived from parameters (CD_1=0.38; B_1=3.2; CD_2=0.43, B_2=1) and Equation (3). Note that the difference between experiment and calculation is 1%, which is within the standard deviation of our measurement. A cluster density measurement under polarized excitation/perpendicular detection yielded a value of 0.635 clusters/beam area. Assuming population 1 is polarized (r=0.4; CD_1=0.33; B_1=1.9) and population 2 is depolarized (r=0; CD_2=0.37, B_2=1) we calculate a cluster density of 0.641 clusters/beam area, again within 1% of the experimental value, using equations 3 and 8. Significantly if we assumed population 1 was depolarized (r=0; CD_1=0.33; B_1=3.2) and population 2 polarized (r=0.4; CD_2=0.37, B_2=0.6) we calculate a cluster density of 0.469 clusters/beam area. If both populations were equally polarized (CD_1=0.33; B_1=3.2; CD_2=0.43, B_2=1), we calculate a cluster density of 0.548 clusters/beam area. Thus qualitatively, at least, a model with a polarized bright population and a depolarized dim population, is consistent with the apparent cluster densities acquired from conventional (unmodulated) fluorescence image of the beads.

A comparison can also be made between the extracted lifetimes from the phase-sensitive fluorescence ICS analysis and a two-component lifetime model from FLIM image of the beads sample [12–14]. Using the polar plot feature in the LIFA software, and assuming only 2 lifetime states in the system, the extracted lifetimes were in the ranges 3.96-3.98 ns and 16.2-21.8 ns (range represent different intensity threshold settings). These estimates agree to within 20% of the lifetimes 3.9 ns and 19.4 ns determined with the phase-sensitive ICS approach. We note that the longer lifetime estimate is somewhat dependent on the choice of intensity threshold when analyzing the FLIM data-this appears to be a trade-off between improving signal to noise (higher threshold) and including the dimmer states (lower threshold). In the phase sensitive fluorescence ICS approach, no manual thresholds were applied.

It is instructive to compare the results using our frequency-domain approach with the more conventional and intuitive time resolved anisotropy decay. For this purpose, we simulated the anisotropy decay curve of the associative system. To do this we use the more general formula [31] for the anisotropy decay of a two-population system, as r(t),

$$r(t)=(I_1(t)r_1(t)+ I_2(t)r_2(t))/(I_1(t)+ I_2(t)) \quad (11)$$

Equation (10) can be rewritten in terms of the parameters in this study, Equation (11).

$$r(t)=N(t)/D(t)$$

$$N(t)=[CD_1B_1\exp(-t/\tau_1)r0_1\exp(-t/\phi_1) +CD_2B_2 \exp(-t/\tau_2)r0_2\exp(-t/\phi_2)]$$

$$D(t)=CD_1B_1\exp(-t/\tau_1) + CD_2B_2\exp(-t/\tau_2) \quad (12)$$

Figure 8 depicts a simulation using Equation (11) using the parameters extracted from the polarized phase sensitive fluorescence ICS. The anisotropy decays from an initial value of 0.3 to nearly zero over a time range of tens of nanoseconds. A rough estimate of the average, apparent correlation time from this plot is about 10 ns.

 doi:10.20944/preprints202603.0322.v1

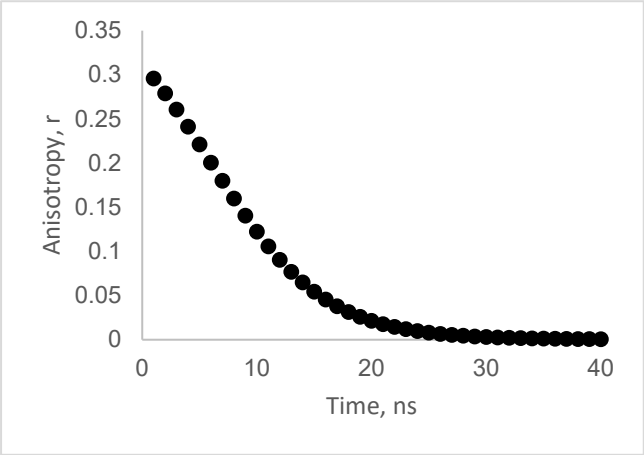

Figure 8. Anisotropy decay simulated from the 2-population associative model assuming spatial averaging. Note that the associative model predicts an apparent anisotropy decay on the scale of nanoseconds, even though both populations are immobile. The plot was generated using Equation (11) with parameters (CD_1=0.38; B_1=3, τ=3.9 ns, r_{01}=0.4, ϕ_1=10000 ns); population 2(CD_2=0.42, B_2=1, τ=19.4 ns, r_{02}=0, ϕ_2=10000 ns).

4. Discussion

The goal of quantitative image analysis, seen from a molecular spectroscopy point of view, is to determine the molecular concentrations (or densities) of different states (defined by excited-state decay rates and diffusion parameters) and in systems undergoing molecule-molecule interactions, the association states (brightness). Imaging alone or time-resolved spectroscopy alone cannot address all these requirements. Image population distribution is measured by pixel count, while time-resolved spectroscopy without spatial resolution provides data as photon counts per state.

The philosophy presented in this paper is to view an image of fluorescent particles as a spatial record of fluctuations. In this approach the concentration and brightness information is determined from a spatial autocorrelation analysis of the images. This is the image correlation spectroscopy approach originally conceived and applied by Peterson and Wiseman [2–9]. By adding polarized illumination, modulated excitation, modulated and polarized detection, phase-sensitive fluorescence images can be created that encode information on the excited-state and rotational rates. Image correlation analysis on the polarization and phase-sensitive fluorescence images can then be fit to a model for the underlying states in terms of concentration, brightness, lifetime and correlation time.

The output from polarized phase sensitive fluorescence image correlation spectroscopy is the (apparent) cluster density as a function of (detector) phase. A 3D dataset (I(x,y), phase) is collapsed onto a 2D plot (CD, phase). The information gleaned from the plot is directly related to the heterogeneity in population and/or polarization decay rates (lifetimes and correlation times). A CD independent of phase implies homogeneity of lifetimes in the image, while a CD versus phase plot that shows a distinct dip [30] or peak (this work) implies a heterogenous lifetime system. Heterogeneity in rotational motion can be manifest in changes to the shape (broadening, peak splitting) and/or amplitude of the CD_{perp} versus phase plots relative to the unpolarized conditions.

When tested on a model fluorescence system-fluorescent beads dispersed on microscope slide-clear evidence for lifetime heterogeneity was obtained. In the context of an admittedly simple two-population model we were able to extract the cluster densities and relative brightness of the two lifetime states. Extension to polarized excitation/perpendicular polarized detection enabled distinction between different correlation time models. Non-associative models (rotational motions common to both populations) could be clearly excluded in the analysis. An associative model with a highly polarized emission linked to one state and a highly depolarized emission linked to the other state was seen to be the best of the models tested.

It is important to discuss the advantages and limitations of the method presented here. The advantages and limitations of ICS are well understood from the papers from the Wiseman laboratory.

 doi:10.20944/preprints202603.0322.v1

Averaging over many fluctuations over a large area results in a robust estimate for particle densities [7]. Our replicate measurements on the fluorescent bead samples yielded standard deviations of 0.005 for cluster densities of the order of 0.5 clusters/beam area or about 1% coefficient of variation (120 separate measurements). Because fluorescent beads are ideal samples, the standard deviation reported here is likely to be a lower limit and thus an overestimate on the precision. The key assumption in the method presented here is that the actual density of particles is independent of the detector phase and that the brightness of different dynamic states is modulated with the detector phase depending on the lifetime and/or correlation time characteristics. In principle particle motion, photobleaching or photo-induced lifetime or rotation would invalidate the assumptions presented above. Particle motion due to diffusion will produce fluctuations in the particle occupancy numbers in the image. However, depending on the particle density and the image size, these fluctuations can be estimated and considered in the analysis. Photobleaching will reduce intensities and cluster densities [32]. This can be estimated using an unmodulated sample and corrected in the analysis [32]. Photoconversion leading to changes in lifetime can be determined using standard lifetime measurements. We note that the assumptions in our method are less stringent than the assumptions made in camera-based fluorescence lifetime imaging microscopy. In FLIM the assumption is that the number of molecules per pixel does not change during image acquisition, whereas in our method the assumption is that the total number of particles per imaging area remains constant during image acquisition.

Regarding the polarized measurements, the approach to compute the cluster density under polarized excitation/perpendicular polarized detection is, to the best of our knowledge, novel. An advantage of using ICS is that it eliminates the need to measure a G-factor. This is primarily because the cluster density is computed as a relative squared fluctuation and is independent of the absolute signal intensity. Likewise, the phase and modulation are also parameters that are independent of signal. Our method does not require calculations of anisotropy, phase difference or modulation ratios that are conventionally used in frequency-domain anisotropy decay measurements [24–27]. The anisotropy, difference phase between parallel and perpendicular components of the emission, and the AC ratio between parallel and perpendicular components have been used as parameters to construct rotational correlation time images [24]. In contrast, our method seeks to provide a state representation of species in an image based on only a few components (cluster density, brightness, lifetime, correlation time). Once the state representation is established, the spatial distribution of these different states can be mapped into an image. For example, in the context of associative lifetime-correlation time models, the phasor plot (or polar or AB plot) can be used to create images based on the fractional fluorescence of different lifetime states. Because of the lifetime-correlation time association, these images could then be used to create rotational correlation time images.

We envisage a range of biological applications in which the polarized-phase-sensitive fluorescence ICS could be employed. Dyes [33–36], which can display environment sensitive fluorescence often have different lifetimes depending on environment. Moreover, dyes can partition into domains, membranes, organelles [33] or even cells depending on biological/biophysical states [33–36]. This partition can create local structures with widely varying brightness and density. The partitioning or binding can also lead to a decrease in rotational diffusion or an increase in depolarization if dyes are packed together and undergo energy migration. Biological macromolecules often exhibit a complex “lifestyle” in the cellular environment. Interactions with other molecules can lead to altered lifetimes and correlation times, and self-association or localization in domains can lead to increases in brightness and/or density. FRET is another potential application [37–40]. FRET results in a decrease in the lifetime and quantum-yield of the excited donor when it transfers non-radiatively to the acceptor. If FRET results from the interaction of one molecule with another, an increase in rotational correlation time of the donor should be observed due to the slower tumbling of the complex. Thus molecule-molecule interactions can be probed with greater detail given brightness, lifetime and rotational correlation time information.

 doi:10.20944/preprints202603.0322.v1

5. Conclusions

A novel extension to ICS, called polarized-phase-sensitive fluorescence ICS, was presented. Use of polarized excitation and perpendicular detection as well as phase-sensitive detection allow fluorescence from species with different lifetime or rotational correlation time to be enhanced or diminished. Analysis of the fluctuations in space of images collected as a function of polarization state and phase can reveal the densities, relative brightness, lifetimes and correlation times of different states. A two-population model was simulated showing qualitatively differing behavior depending on model complexity. Application to an experimental sample mimicking domains or oligomerization revealed distinct coupling between brightness, lifetime and correlation time.

Funding: This research received no external funding.

Acknowledgments: The authors have reviewed and edited the output and take full responsibility for the content of this publication.

Conflicts of Interest: The authors declare no conflicts of interest.

Abbreviations

The following abbreviations are used in this manuscript:

FLIM	Fluorescence lifetime imaging microscopy
ICS	Image Correlation Spectroscopy
CD	Cluster Density
B	Brightness

Appendix A

Appendix A.1

In this appendix, formulae pertaining to FLIM and FLIM with polarized excitation/perpendicular detection is outlined. We begin with the simplest form of intensity decay, namely single exponential decay, characterized with lifetime, τ.

$$I(t)=I_o \exp(-t/t) \quad (A1)$$

To represent the intensity decay in the frequency domain it is convenient to compute the sine and cosine transforms of the intensity decay given in Equation (A1).

$$M\cos(F)=\int I(t) \cos(wt)\, dt/\int I(t)\, dt=1/(1+(wt)^2 \quad (A2)$$

$$M\sin(F)=\int I(t) \sin(wt)\, dt/\int I(t)\, dt= wt\ /(1+(wt)^2 \quad (A3)$$

where w is the modulation frequency.

If the intensity decay, I(t) is more complex, i.e., two components, with lifetimes t_1 and t_2 and associated amplitudes A_1 and A_2,

$$I(t)=I_o (A_1 \exp(-t/t_1) + A_2 \exp(-t/t_2) \quad (A4)$$

Then the sine and cosine transforms become,

$$M\cos(f)=\int I(t) \cos(wt)\, dt/\int I(t)\, dt=a/(1+(wt_1)^2)+(1-a)/(1+(wt_2)^2) \quad (A5)$$

$$M\sin(f)=\int I(t) \sin(wt)\, dt/\int I(t)\, dt= a\ wt_1\ /(1+(wt_1)^2)+(1- a)\ wt_2\ /(1+(wt_2)^2) \quad (A6)$$

In equations A5 and A6 the fractions of the two states are expressed as fractional fluorescence, $a=(A_1t_1)/(A_1t_1+ A_2t_2)$.

 doi:10.20944/preprints202603.0322.v1

Now we consider the situation of polarized excitation with perpendicular polarized emission. The intensity decay is now influenced by the decay of the excited state I(t) and the decay of anisotropy, r(t). The perpendicular-polarized component of the emission is given by $I_{perp}(t)$,

$$I_{perp}(t)=(1/3)\, I(t)\, (1-r(t)) \quad (A7)$$

If we assume the simplest form of anisotropy decay, r(t), characterized with a rotational correlation time f and an initial, zero-time anisotropy of r_0,

$$r(t)=r_0 \exp(-t/f) \quad (A8)$$

Then $I_{perp}(t)$ takes on the form as a double exponential decay in time,

$$I_{perp}(t)=(1/3)\, I_o\, ((\exp(-t/t) - r_o \exp(-t/t_2)) \quad (A9)$$

Where $t_2= t/(1+(t/f))$

The cosine transform and sine transform of the perpendicular-polarized component of the emission are given by Equations (A5) and (A6), with $t_2= t/(1+(t/f))$ and $a= t/(t- r_o\, t_2)$;$(1-a)=-r_0\, t_2/(t- r_o\, t_2)$.

To connect the cosine transform and sine transforms to the phase-sensitive fluorescence ICS and polarized phase-sensitive ICS, we make use of the trigonometric identity,

$$\cos(x-a)=\cos(x)\cos(a)+\sin(x)\sin(a) \quad (A10)$$

Substituting Equation (A10) into Equation (5) from the main text we obtain,

$$Bi(\vartheta)=B_i\, (1+ m\cos(\Phi_i-\vartheta))= B_i(1+m\cos(\Phi)\cos(\vartheta)+m\sin(\Phi)\sin(\vartheta)) \quad (A11)$$

References

1. Magde, D., E. L. Elson, and W. W. Webb. 1972. Thermodynamic fluctuations in a reacting system: measurement by fluorescence correlation spectroscopy. Phys. Rev. Lett. 29:705–708.
2. Petersen, N. O. 1986. Scanning fluorescence correlation spectroscopy. I. Theory and simulation of aggregation measurements. Biophys. J. 49:809–815.
3. St-Pierre, P. R., and N. O. Petersen. 1990. Relative ligand binding to small or large aggregates measured by scanning correlation spectroscopy. Biophys. J. 58:503–511.
4. Petersen, N. O., P. L. Hoddelius, P.W. Wiseman, O. Seger, K. E. Magnusson. 1993. Quantitation of membrane receptor distributions by image correlation spectroscopy: concept and application. Biophys. J. 65:1135–1146.
5. Wiseman, P. W., and N. O. Petersen. 1999. Image correlation spectroscopy. II. Optimization for ultrasensitive detection of preexisting platelet-derived growth factor-β receptor oligomers on intact cells. Biophys. J. 76:963–977.
6. Petersen, N. O., C. Brown, P. W. Wiseman. 1998. Analysis of membrane protein cluster densities and sizes in situ by image correlation spectroscopy. Faraday Discuss. 111:289–305.
7. Costantino, S., J. W. Comeau, P. W. Wiseman. 2005. Accuracy and dynamic range of spatial image correlation and cross-correlation spectroscopy. Biophys. J. 89:1251–1260.
8. Comeau, J. W., D. L. Kolin, and P. W. Wiseman. 2008. Accurate measurements of protein interactions in cells via improved spatial image cross-correlation spectroscopy. Mol. Biosyst. 4:672–685.
9. Hebert, B., S. Costantino, and P. W. Wiseman. 2005. Spatiotemporal image correlation spectroscopy (STICS) theory, verification, and application to protein velocity mapping in living CHO cells. Biophys. J. 88:3601–3614.
10. Lakowicz, J.R. and Berndt, K.W. 1991. Lifetime selective fluorescence imaging using an rf phase sensitive camera. Rev. Sci. Instrum. 62, 1727; doi: 10.1063/1.1142413
11. Datta R, Heaster TM, Sharick JT, Gillette AA, Skala MC. Fluorescence lifetime imaging microscopy: fundamentals and advances in instrumentation, analysis, and applications. J Biomed Opt. 2020 May;25(7):1-43. doi: 10.1117/1.JBO.25.7.071203. PMID: 32406215; PMCID: PMC7219965.

 doi:10.20944/preprints202603.0322.v1

12. Clayton AH, Hanley QS, Verveer PJ. Graphical representation and multicomponent analysis of single-frequency fluorescence lifetime imaging microscopy data. J Microsc. 2004 Jan;213(1):1-5. doi: 10.1111/j.1365-2818.2004.01265.x. PMID: 14678506.
13. Redford GI, Clegg RM. Polar plot representation for frequency-domain analysis of fluorescence lifetimes. J Fluoresc. 2005 Sep;15(5):805-15. doi: 10.1007/s10895-005-2990-8. PMID: 16341800.
14. Digman MA, Caiolfa VR, Zamai M, Gratton E. The phasor approach to fluorescence lifetime imaging analysis. Biophys J. 2008 Jan 15;94(2):L14-6. doi: 10.1529/biophysj.107.120154. Epub 2007 Nov 2. PMID: 17981902; PMCID: PMC2157251.
15. Vallmitjana A, Torrado B, Dvornikov A, Ranjit S, Gratton E. Blind Resolution of Lifetime Components in Individual Pixels of Fluorescence Lifetime Images Using the Phasor Approach. J Phys Chem B. 2020 Nov 12;124(45):10126-10137. doi: 10.1021/acs.jpcb.0c06946. Epub 2020 Nov 3. PMID: 33140960; PMCID: PMC9272785.
16. Oleksiievets N, Thiele JC, Weber A, Gregor I, Nevskyi O, Isbaner S, Tsukanov R, Enderlein J. Wide-Field Fluorescence Lifetime Imaging of Single Molecules. J Phys Chem A. 2020 Apr 30;124(17):3494-3500. doi: 10.1021/acs.jpca.0c01513. Epub 2020 Apr 17. PMID: 32255633.
17.] Weber G 1952 Polarization of the fluorescence of macromolecules. I. Theory and experimental method Biochem. J. 51 145–55
18. Weber G 1952 Polarization of the fluorescence of macromolecules. II. Fluorescent conjugates of ovalbumin and bovine serum albumin Biochem. J. 51 155–67
19. Porter G, Sadkowski P J and Treadle C J 1977 Picosecond rotational diffusion in kinetic and steady-state fluorescence spectroscopy Chem. Phys. Lett. 49 416–20
20. Spencer R D and Weber G 1970 Influence of Brownian rotations and energy transfer upon the measurements of fluorescence lifetime J. Chem. Phys. 52 1654
21. Cross A J and Fleming G R 1984 Analysis of time-resolved fluorescence anisotropy decays Biophys J. 46 45–56
22. Lakowicz J R, Cherek H, Maliwal B P and Gratton E 1985 Time resolved fluorescence anisotropies of diphenylhexatriene and perylene in solvents and lipid bilayers obtained from multifrequency phase-modulation fluorometry Biochemistry 24 376–83
23. Siegel J, Suhling K, French P M W, Phillips D, Davis D M, Webb S E D, Sabharwal Y and Levequefort S 2003 Wide-field time-resolved fluorescence anisotropy imaging (TR-FAIM): imaging the rotational mobility of a fluorophore Rev. Sci. Instrum. 74 182–92
24. Clayton A H A, Hanley Q S, Arndt-Jovin D J, Subramaniam V and Jovin T M 2002 Dynamic fluorescence anisotropy imaging microscopy in the frequency domain (rFLIM) Biophys. J. 83 1631–49
25. Weber G 1977 Theory of differential phase fluorometry: detection of anisotropic molecular rotations J. Chem. Phys. 66 4081–91
26. Lakowicz J R and Prendergast F G 1978 Quantitation of hindered rotations of diphenylhexatriene in lipid bilayers by differential polarized phase fluorometry Science 200 1399–401
27. Weber G, Helgerson S L, Cramer W A and Mitchell G W 1976 Changes in rotational motion of a cell-bound fluorophore caused by colicin E1: a study by fluorescence polarization and differential polarized phase fluorometry Biochemistry 15 4429–32
28. Kozer N and Clayton AHA 2016. Analysis of complex anisotropy decays from single-frequency polarized-phasor ellipse plots. *Methods Appl. Fluoresc.* **4** 024005 DOI 10.1088/2050-6120/4/2/024005
29. Kozer N, Clayton AHA 2020. In-cell structural dynamics of an EGF receptor during ligand-induced dimer-oligomer transition. Eur Biophys 49(1):21-37. doi: 10.1007/s00249-019-01410-2.
30. Clayton AHA 2024. Phase-Sensitive Fluorescence Image Correlation Spectroscopy. Int J Mol Sci. 25(20):11165. doi: 10.3390/ijms252011165.
31. Smith TA, Ghiggino KP 2015. A review of the analysis of complex time-resolved fluorescence anisotropy data. Methods Appl Fluoresc. 3(2):022001. doi: 10.1088/2050-6120/3/2/022001.
32. O Ciccotosto GD, Kozer N, Chow TT, Chon JW, Clayton AH 2013. Aggregation distributions on cells determined by photobleaching image correlation spectroscopy. Biophys J. 2013 Mar 5;104(5):1056-64. doi: 10.1016/j.bpj.2013.01.009.ur

 doi:10.20944/preprints202603.0322.v1

33. Klymchenko AS 2023. Fluorescent Probes for Lipid Membranes: From the Cell Surface to Organelles. Acc Chem Res. Jan3 56(1):1-12. doi: 10.1021/acs.accounts.2c00586.
34. Steinmark IE, James AL, Chung PH, Morton PE, Parsons M, Dreiss CA, Lorenz CD, Yahioglu G, Suhling K. 2019. Targeted fluorescence lifetime probes reveal responsive organelle viscosity and membrane fluidity. PLoS One. Feb 14;14(2):e0211165. doi: 10.1371/journal.pone.0211165.
35. Lira RB, Dillingh LS, Schuringa JJ, Yahioglu G, Suhling K, Roos WH. 2024. Fluorescence lifetime imaging microscopy of flexible and rigid dyes probes the biophysical properties of synthetic and biological membranes. Biophys J. Jun 18;123(12):1592-1609. doi: 10.1016/j.bpj.2024.04.033.
36. Lim C, Seah D, Vendrell M. Chemical fluorophores for fluorescence lifetime imaging 2026. Chem Soc Rev. 2026 Feb 9;55(3):1352-1370. doi: 10.1039/d5cs00280j.
37. Long, Y., Stahl, Y., Weidtkamp-Peters, S. et al. In vivo FRET–FLIM reveals cell-type-specific protein interactions in Arabidopsis roots. Nature 548, 97–102 (2017). https://doi.org/10.1038/nature23317
38. Jares-Erijman, E., Jovin, T. FRET imaging. 2003. Nat Biotechnol 21, 1387–1395. https://doi.org/10.1038/nbt896
39. Weber, A., Hartig, R. & Zuschratter, W. (2025). FRET-analysis in living cells by fluorescence lifetime imaging microscopy: experimental workflow and methodology. Methods in Microscopy, 2(1), 73-84. https://doi.org/10.1515/mim-2024-0027
40. Berezin MY, Achilefu S. Fluorescence lifetime measurements and biological imaging. Chem Rev. 2010 May 12;110(5):2641-84. doi: 10.1021/cr900343z.